ADVANCES IN MATERIALS AND PROCESSING TECHNOLOGIES
https://doi.org/10.1080/2374068X.2021.1949175

Taylor & Francis
Taylor & Francis Group

RESEARCH ARTICLE

Check for updates

ɤ-TiAl alloy: revisiting tensile creep deformation behaviour and creep life at 832 °C

Mainak Saha

Department of Metallurgical and Materials Engineering, National Institute of Technology (NIT), Durgapur, West Bengal, India

ABSTRACT

Creep deformation in single-phase ɤ-TiAl alloys manufactured using different processing techniques has been an extensively studied topic owing to the high specific strength and excellent creep properties of these alloys at temperatures between 760 and 1000°C. In addition, these lightweight and creep-resistant alloys are being presently considered as replacements to the comparatively heavier Ni-based superalloys for application in the low-pressure turbine blades of the next-generation gas turbine engines. However, there is limited information on the tensile creep deformation behaviour and creep life of ɤ-TiAl alloys at 832°C where these alloys have been reported not to exhibit steady-state creep. To this end, the present work revisits the work on understanding the tensile creep deformation behaviour of wrought single-phase ɤ-TiAl alloy by Saha [1] and is aimed to develop an understanding of the tensile creep deformation behaviour at 832°C and the influence of creep activation energy on the creep life of wrought single-phase ɤ-TiAl alloy for stress levels of 69.4 and 103.4 MPa at 832°C using Monkman–Grant [2] approach.

ARTICLE HISTORY
Accepted 25 June 2021

KEYWORDS
-TiAl; Monkman–Grant parameter; Coble creep; Nabarro–Herring creep; superdislocation; dislocation; Kuhlmann-Wilsdorf barrier

1. Introduction

Near γ-titanium aluminide (TiAl) alloys offer a range of attractive properties such as high specific strength and good high-temperature properties which include high oxidation resistance and good creep resistance [1]. In addition, single-phase γ-TiAl alloys exhibit much better fracture toughness and creep resistance as compared to that of near γ-TiAl alloys [2]. This makes single-hase γ-TiAl alloys potential candidates for the replacement of the much heavier Ni-based superalloys in the low-pressure turbine blades of the next-generation gas turbine engines in aircrafts. On the other hand, the creep activation energies from both bulk and grain boundaries (GBs) simultaneously influence the creep life of the material for high-temperature applications [3]. This necessitates extensive creep studies primarily focusing on the influence of tertiary creep and creep activation energy on the creep life of these materials. A series of reports on the room temperature tensile deformation behaviour of single-phase ɤ-TiAl alloys ($L1_0$ structure) show that the near-ɤ, two phase compositions having ~ 48 at.% Al possess very high

CONTACT Mainak Saha mainaksaha1995@gmail.com Department of Metallurgical and Materials Engineering, National Institute of Technology (NIT), Durgapur, West Bengal 713209, India

© 2021 Informa UK Limited, trading as Taylor & Francis Group

Electronic copy available at: https://ssrn.com/abstract=4067222

toughness (ultimate tensile strength ~844–1010 MPa and tensile ductility ~3–4.6% at room temperature) [4–7]. Extensive creep deformation studies have been carried out on a number of two phase near-ɣ-TiAl alloys produced by various processing routes [4,8]. In addition, compression creep-based investigations have been performed on a number of single-phase ɣ-TiAl alloys and a number of literatures have reported that minimum strain rates during creep testing at different regimes of temperature and stress hugely influence the grain size of single-phase ɣ-TiAl alloys (during creep testing) [3,9,10]. Minimum strain rate of such intermetallic-based alloys may be defined in terms of Mukherjee–Bird–Dorn (MBD) equation [11–13].

Hayes and Martin [4] have presented an analysis of the minimum strain rate deformation of a wrought single-phase ɣ-TiAl alloy within temperature range of 760–1000°C and stress range of 32–345 MPa. In addition, the aforementioned work [4] also predicts the main mechanism for creep rupture at different temperatures, in a given stress range, using Larson–Miller (L-M) [14] and Monkman–Grant (M-G) plots [15] and extensive microstructural characterisation using optical microscope (OM) and the transmission electron microscope (TEM). Besides, a recent report (from the author) on the tensile creep deformation behaviour of ɣ-TiAl has determined the stress exponent and creep activation energies between 760 and 900°C at 69.4 and 103.4 MPa [16]. Moreover, based on creep activation energies and stress exponents, it has been reported that there is a transition from dislocation-glide to dislocation-climb controlled creep at very low creep stress levels (~66.68 MPa) [16] and that there is steady-state creep observed for both interrupted and uninterrupted creep tests at 832°C [4]. A previous work by the author [16] has refuted some of the major observations of the earlier work by Hayes and Martin [4] which are:

- There is no tertiary creep between 760 and 900°C, at stress levels of 69.4 and 103.4 MPa in wrought single-phase ɣ-TiAl alloy.
- Steady-state creep is observed at 832°C, at stress levels of 69.4 MPa, for both interrupted and uninterrupted tests.
- Single-phase ɣ-TiAl alloy does not exhibit dislocation creep at 760, 832 and 900°C and at stress levels between 32 and 345 MPa.

Moreover, there is limited understanding of creep behaviour and creep rupture life as a function of stress at 832°C. To this end, the present work is aimed towards understanding the creep deformation behaviour at 832°C and the influence of creep activation energies on the rupture life (of the material) for stress levels of 69.4 and 103.4 MPa at 832°C using M-G approach. 832°C has been chosen as the creep test temperature and 69.4 and 103.4 MPa have been chosen as the creep stress levels since the creep behaviour and the influence of creep activation energies on the creep life at the aforementioned temperature and stress levels are not known till date. The approach used in the present work is the determination of tensile creep deformation behaviour from strain rate vs. strain plots at 832°C followed by the determination of creep life for two different stress levels (69.4 and 103.4 MPa) using M-G approach and finally correlating the creep activation energies using Ashby's approach [17] for both GB diffusion creep (or Coble creep) and lattice diffusion creep [or Nabarro–Herring (NH) creep] with the overall creep life (of ɣ-TiAl alloy) at 69.4 and 103.4 MPa at 832°C .

Electronic copy available at: https://ssrn.com/abstract=4067222

2. Theoretical analysis

Based on the single-phase ɤ-TiAl alloy composition and tensile creep test parameters used by Saha [16], the minimum strain rate (ε_{min}) vs. strain (ε) and ln(ε_{min}) vs. ε plots have been determined at 832°C for two different stress levels, viz., 69.4 and 103.4 MPa for the purpose of understanding the influence of creep stress and temperature on the three creep regimes (viz., primary, secondary and tertiary) and the influence of the same on the creep life of the material. For creep life determination, M-G approach was used. For M-G approach, the governing equation is [3,18]

$$\overset{t_r}{\varepsilon_s} = C_{MG} \tag{2}$$

where, ε_s is the steady-state creep rate (~ ε_{min} based on the justification that many metallic materials may not exhibit steady-state creep (provided in ref [16].)), t_r is the rupture time (expressed in seconds) and C_{MG} (~1.40 at 832°C) is the M-G constant (obtained from ref [16].).

3. Results

Figure 1(a,b) shows the variation of $\underline{\varepsilon}$ with ε (in both linear and logarithmic scales, respectively) for three cases, viz., uninterrupted creep testing and interrupted creep testing with termination strains of 0.18 and 0.5%. Figure 1(b) shows the creep regimes at 832°C (for stress levels of 69.4 and 103.4 MPa, respectively) with a higher simplicity. Based on Figure 1, it is observed that the present material (45.9Ti–0.91Nb–52.9Al (at.%)) shows a very early onset of tertiary creep at 832°C for uninterrupted creep test and for creep test terminated at 0.5% strain, whereas there is no primary (or transient) creep observed during creep test interrupted at strain of 0.18% (Figure 1), indicating that the material (used in the present work) does not exhibit resistance to creep deformation for the aforementioned deformation condition. Besides there is a limited regime of tertiary

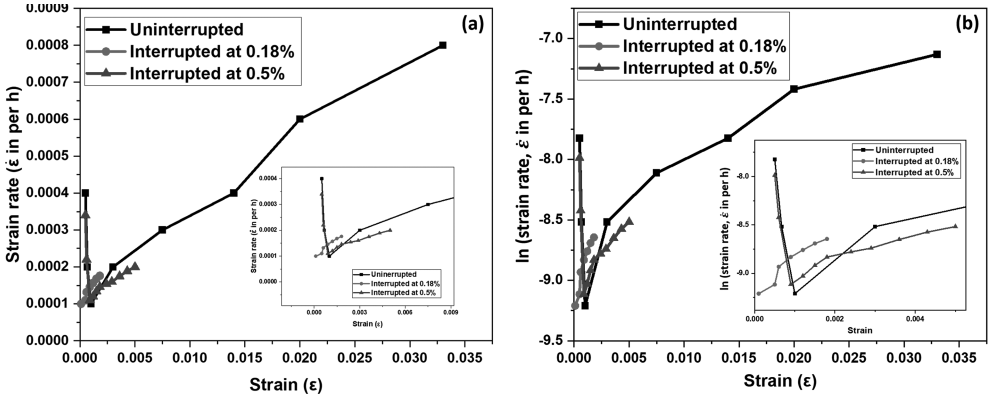


Figure 1. Variation of (a) $\underline{\varepsilon}$ with ε, and (b) ln($\underline{\varepsilon}$) with ε. In parts (a) and (b), the plot uninterrupted creep test has been represented using black colour, whereas the creep tests terminated at 0.18% and 0.5% have been represented using red and blue colours, respectively. The inset images in parts in (a) and**(b)** represent the different creep regimes in both interrupted and uninterrupted creep tests with a high level of clarity (reproduced with permission from ref [16]).

Electronic copy available at: https://ssrn.com/abstract=4067222

creep observed for creep tests terminated a 0.18% and 0.5% strain (Figure 1). In addition, the material shows a dominant tertiary creep regime for the case of uninterrupted tensile creep testing (Figure 1). Secondary (or steady-state creep) is not observed in any case (Figure 1). In other words, the interrupted creep tests lead to a higher rate of vacancy formation at GBs normal to the tensile stress subsequently followed by void growth and coalescence, leading to an intergranular fracture, as mentioned in refs. [19–21]. Explanation of the above tendencies during interrupted and uninterrupted tensile creep test (at 832°C) is subject to extensive microstructural investigations which is beyond the scope of the present discussion.

For uninterrupted creep testing, there is a dominant tertiary creep regime (Figure 1). Moreover, it has been reported that the extent of tertiary creep hugely influences the creep life of the material [20,22–24]. To this end, creep life determination has been performed for samples (with uninterrupted creep testing) at 832°C. Figure 2 shows the creep life plots (for uninterrupted creep testing) based on M-G approach for stress levels of 69.4 and 103.4 MPa at 832°C. From Figure 2, it is observed that t_r decreases with increasing $\underline{\varepsilon}_{min}$ at 832°C (based on equation 2). Moreover, the slope (p) of the M-G curve (in Figure 2) is calculated as −1.33 which suggests that the mechanism of creep rupture is power-law breakdown at 832°C (using the criteria mentioned in refs. [3,25–30]). Hayes and Martin [4] and Saha [16] have reported that $\underline{\varepsilon}_{min}$ decreases with increasing stress levels (from 69.4 to 103.4 MPa) at 832°C. Moreover, Saha [16] has reported that the creep mechanisms operating at different stress levels (69.4 and 103.4 MPa) at 832°C are independent of each other and, hence, are not sequential. Hence, combining the trend observed between $\underline{\varepsilon}_{min}$ with t_r (Figure 2) with the aforementioned reports ([4,16]), it may be inferred that M-G-based approach to determine the creep life also predicts that t_r decreases with increasing stress levels (from 69.4 to 103.4 MPa) at 832°C.

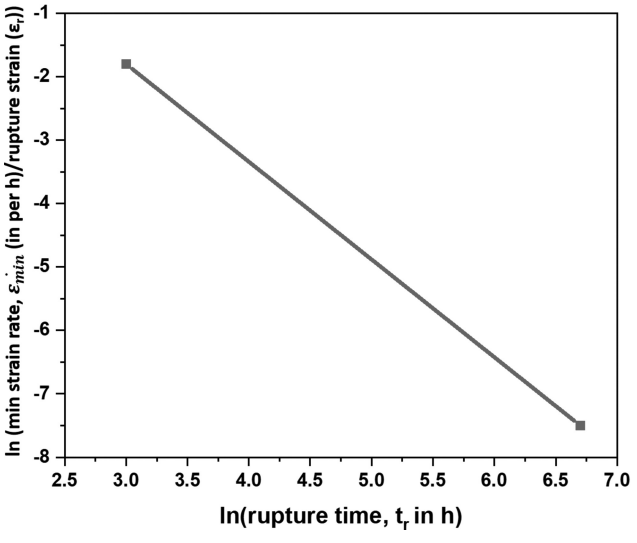


Figure 2. M-G plots for determining creep life for 69.4 and 103.4 MPa at 832°C. $\underline{\varepsilon}_{min}$ has been normalised with rupture strain (ε_r) determined from Figure 1. A justification of the above normalisation (for M-G plots) has been provided in ref [14].

Electronic copy available at: https://ssrn.com/abstract=4067222

Table 1. Coble and Nabarro–Herring (NH) creep activation energies ($Q_{GB}$and Q_l, respectively) for stress levels of 69.4 and 103.4 MPa at 832°C [16].

Stress level (MPa)	Test temperature (°C)	Coble creep activation energy (Q_{GB}) (kJ/mol)	Nabarro–Herring creep activation energy (Q_l) (kJ/mol)
69.4	832	210	350
103.4	832	151.88	253.13

Based on the Ashby's model [25], the constitutive equation for NH (or lattice diffusion creep) is given as

$$\dot{\varepsilon} = 9.3\frac{D_l G b}{kT}\left(\frac{b}{d}\right)^2\left(\frac{\sigma}{G}\right) \tag{3}$$

where $\dot{\varepsilon}$ is the strain rate, D_l is the lattice diffusivity, b is the Burgers vector, d is the grain size, k is the Boltzmann constant, σ is the creep stress and G is the shear modulus of the material. Similarly, using Ashby's model, the constitutive equation for Coble creep (or GB diffusion creep) is given as

$$\dot{\varepsilon} = 33.4\frac{D_{GB} G b}{kT}\left(\frac{b}{d}\right)^3\left(\frac{\sigma}{G}\right)\left(\frac{\delta}{b}\right) \tag{4}$$

where is the GB width and D_{GB} is the activation energy for GB diffusion. Both D_{GB} and D_l are highly temperature-dependent [25]. However, the magnitude of D_{GB} is higher than that of D_l at lower homologous temperatures, whereas the magnitude of D_l is higher than that of D_{GB} at higher homologous temperatures [31,32]. This is because GBs offer a higher pathway for diffusion at lower temperatures when compared with that of the lattice [33]. Moreover, a comparison of equations (3) and (4) shows that Coble creep has a higher grain-size dependence as compared to that of NH creep. In other words, although both Coble and NH creep may operate simultaneously, Coble creep is the dominant diffusion creep mechanism for fine grain sizes at lower temperatures whereas NH creep dominates for comparatively coarser grains at higher temperatures. However, both these mechanisms show a similar sensitivity towards σ (as shown in equations (3) and (4)). Based on the previous reports [4,16], d has minimal influence on $\dot{\varepsilon}$. The direct proportionality between $\dot{\varepsilon}$ ad σ in equations (3) and (4) also explains the previous observations (in refs. [4,16,34]) on the increasing magnitude of $\dot{\varepsilon}$ with increasing stress levels from 69.4 to 103.4 MPa. Besides, G, σ, T (~ 832° C) and b are constant in the present work. Table 1 shows the creep activation energy for stress levels of 69.4 and 103.4 MPa at 832°C and has been obtained from ref. [16]. Based on the values of NH and Coble creep activation energies (Q_l and Q_{GB}, respectively) reported for 69.4 MPa (Q_{GB} ~ 210 kJ/mol and Q_l350 kJ/mol at 832°C in ref. [16]) and for 103.4 MPa (Q_{GB} ~ 151.88 kJ/mol and Q_l253.13 kJ/mol at 832°C in ref. [16]), it may be inferred that a decrease in the creep activation energy (for both Coble and NH creep) significantly reduces the creep life of the material with increasing stress levels from 69.4 to 103.4 MPa.

4. Discussion

As highlighted by Lu and Hemker [35], the main deformation mechanisms during tensile creep in absence of steady-state creep at 832 °C are as follows.

Electronic copy available at: https://ssrn.com/abstract=4067222

4.1. Superdislocations

These have been observed in two different forms: (i) formation of fault dipoles and (ii) rectilinear Kuhlmann-Wilsdorf (KW) type of barriers to dislocation motion [36]. For instance, inverse creep in Ni_3Al may be associated with the bowing out of superdislocations and their movement along cube cross-slip plane [37]. Ni_3Al and ɣ-TiAl alloys show similar inverse creep behaviour, suggesting that superdislocation associated deformation behaviour is similar in both Ni_3Al and ɣ-TiAl alloys [35]. Moreover, in both the aforementioned alloys, the disappearance of fault dipoles and linear profile of locked screw superdislocations at later stages of creep deformation suggests that the superdislocation activity only influences the primary creep behaviour in both the aforementioned alloys [35].

Moreover, the drastic decrease in creep rate during primary creep stage for uninterrupted creep test and creep test interrupted at 0.5% strain to failure (Figure 1) may be attributed to the exhaustion of superdislocation movement. For instance, during yielding, the motion of superdislocations has been reported to be inhibited by the two competing mechanisms, viz., (i) Localised pinning and formation of fault dipoles [35] and (ii) global cross slip with formation of KW type of rectilinear barriers [35]. The formation of fault dipoles at lower temperatures has been attributed to the localised pinning of superdislocations followed by the bypassing of pinned segments (of superdislocations) and the subsequent drawing out of fault dipole whose strain energy is reduced by the passage of partial dislocations, leading to the formation of extrinsic stacking faults. The instability of fault dipoles at higher temperatures may be used to understand the temperature dependence of primary creep [35,38]. However, the formation of KW type of barriers has been observed to dominate at higher temperatures and for longer times. Earlier high-resolution transmission electron microscopy (HRTEM) observations [38] have revealed that these barriers undergo dissociation in a nonplanar configuration, and hence, act as very strong obstacles to the further movement of superdislocations.

There is hardly any influence of superdislocation movement on the tertiary creep of ɣ-TiAl alloy as suggested by the macroscopic shape of the creep curves for both uninterrupted and interrupted creep testing (Figure 1). The temperature dependence of tertiary creep has been reported to be comparatively lesser in ɣ-TiAl than that in Ni_3Al. The high temperature dependence of tertiary creep in Ni_3Al has been attributed to the Peierls-like motion of superdislocations on the cube cross-slip plane [35]. Cross-slipped superpartials (or superpartial dislocations) have been observed to be more widely dissociated in ɣ-TiAl than that in Ni_3Al, resulting in a higher Peierls stress for ɣ-TiAl than that in Ni_3Al [35,37]. In this light, the more moderate temperature dependence exhibited by ɣ-TiAl indicates that glide of superdislocations (along cubic {100} plane in ɣ-TiAl) cannot be used to explain tertiary creep in this alloy.

4.2. Ordinary dislocations

The extended nature of tertiary creep that has been shown for the uninterrupted creep test (Figure 1) may be attributed to the increased activity of ordinary dislocations. Although present during primary creep, the importance of ordinary dislocation motion

Electronic copy available at: https://ssrn.com/abstract=4067222

has been reported to occur after a complete exhaustion of superdislocation movement [35]. Pinning and aligning of ordinary dislocations along the screw direction during primary creep suggests that their motion is initially inhibited by the intrinsic process which have been previously used to describe the yield strength anomaly in TiAl. These intrinsic processes involve a double cross-slip phenomenon by which a dislocation undergoes cross-slip to a secondary octahedral slip plane and then comes back to the primary slip system as shown in Figure 3(a-c)) [35]. When a dislocation attains a configuration similar to the one as shown in Figure 3(c) [35], the jogged segment is unable to undergo a forward glide with the remaining part of the dislocation line leading to one of the several non-conservative phenomenon: (i) zipping of the jog (along the lateral direction) leading to the growth of one segment at the expense of the other (Figure 3(d)) [35], (ii) forward climbing of the jog (Figure 3(e)) [35], (iii) pinching off of the leading dislocation leading to a small loop in their neighbourhood (Figure 3(f)) [35] and (iv) spiral motion of the jog segments and their operationas a Z-mill source provided that the jog is sufficiently high (Figure 3(g)) [35].

The increasingly bowed shape of the ordinary dislocations (Figure 3) associated with the latter stages of tensile creep suggests that one or more of the aforementioned processes occur if there is sufficient time allocated for a dislocation at a high homologous temperature [35]. Both the expansion of dislocation loops and the spiralling of a Z-mill source (Figure 3(g)) may lead to an increase in the overall dislocation density [35,39,40]. This may be used to describe the extended tertiary creep regime for controlling the

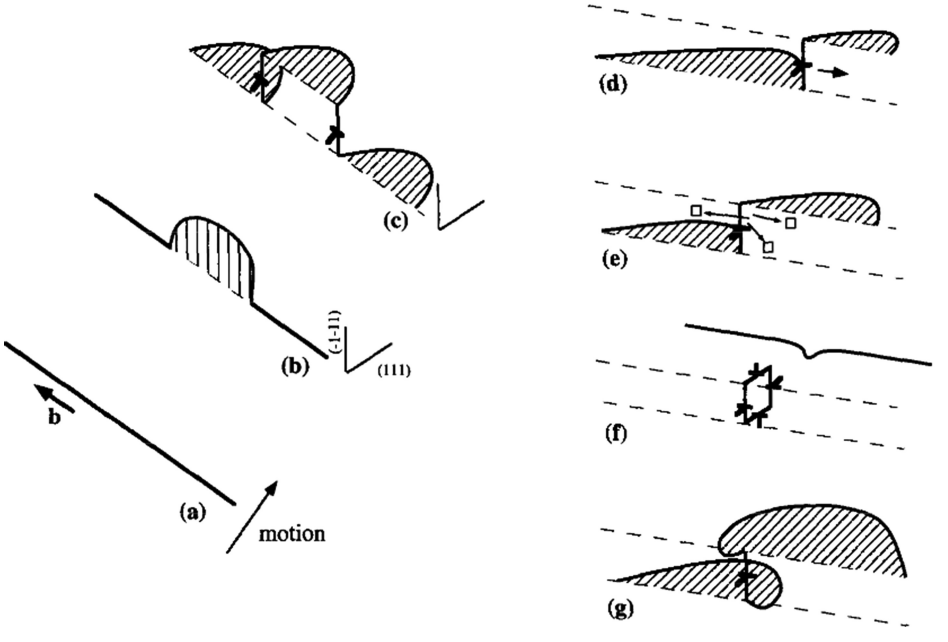


Figure 3. Movement of ordinary dislocation in TiAl: a localised segment of a screw dislocation (a) undergoing cross-slip to a secondary octahedral {111} plane (b) and then comes back to the primary slip plane leading to the formation of (c) two edge segment jogs which cannot undergo glide with the rest of the dislocation (reproduced with permission from ref. [35]).

Electronic copy available at: https://ssrn.com/abstract=4067222

overall creep behaviour during interrupted creep testing of ɤ-TiAl (Figure 1). The role of diffusion in this particular process is clearly understood. The measured creep activation energies at stress levels of 69.4 MPa and 103.4 MPa at 832°C ($Q_{creep} = Q_{GB} + Q_l \sim 560$ kJ/mol at 69.4 MPa, 832°C and 405.01 kJ/mol at 103.4 MPa, 832°C, Q_{GB} and Q_l obtained from Table 1) are much higher than that for diffusion of Ti in TiAl (~ 291 kJ/mol, reported in ref. [35]). The activation energy of Al in TiAl is not accurately measured till date. Q_{creep} becomes important in the context of diffusion creep which requires the diffusion of both Ti and Al in TiAl [40]. Following this principle, Q_{creep} may be related to the climb of jogs at different pinning points. In this context, it is worth mentioning that thermal activation of dislocation motion also plays a key role during diffusion creep in ɤ-TiAl [40]. However, the influence of mechanical twinning (a thermal process) on the dislocation motion at the aforementioned stress and temperature in ɤ-TiAl alloy is yet to be investigated and is beyond the scope of the present discussion.

5. Conclusions

The present work highlights the tensile creep deformation behaviour at 832°C and the influence of creep activation energies (for both Coble and NH creep) on the creep life (of single phase ɤ-TiAl alloy) as a function of increasing stress levels from 69.4 to 103.4 MPa at 832°C (where there is no occurrence of steady-state creep). The approach used in the present work is based on the determination of different creep regimes at 832°C followed by the determination of creep life for two different stress levels (69.4 and 103.4 MPa) using M-G approach and finally correlating the creep activation energies (for both Coble and NH creep) with the overall creep life at 69.4 and 103.4 MPa at 832°C. Moreover, the mechanisms of superdislocation and ordinary dislocation motion operative during tensile creep deformation at the aforementioned stress and temperature have also been elucidated. The following may be concluded based on the results obtained in the present work:

- At 832°C, ɤ-TiAl alloy (45.9Ti–0.91Nb–52.9Al (at.%)) shows a dominant tertiary creep regime for uninterrupted creep testing, whereas there is a limited tertiary creep regime for creep tests (under the same temperature and stresses) for creep tests interrupted at 0.18% and 0.5%, indicating that during interrupted creep testing, there is a higher rate of vacancy formation along GBs normal to the applied tensile stress followed by void coalescence and growth leading to intergranular fracture. Moreover, the dominant creep regime for the uninterrupted creep test at 832°C may be attributed to the increased activity of dislocations during tertiary creep.
- At 832°C for stress levels of 69.4 and 103.4 MPa, a drastic decrease in creep rate with creep strain during primary creep stage for uninterrupted creep test and creep test interrupted at 0.5% of the strain to failure may be attributed to the exhaustion of superdislocation activity during primary creep at the aforementioned temperature and stress levels. Besides, the macroscopic nature of creep curves for both uninterrupted and interrupted creep tests suggests that there is hardly any role of superdislocations on the tertiary creep at the aforementioned temperature and stress levels.

Electronic copy available at: https://ssrn.com/abstract=4067222

- M-G approach (for creep life determination) shows that creep life (for uninterrupted creep testing) decreases with increase in stress levels from 69.4 to 103.4 MPa. In addition, M-G plots indicate the mode of rupture (for uninterrupted creep test) at 832°C (for stress levels of 69.4 and 103.4 MPa) is power-law breakdown.
- A decrease in creep activation energy (for both Coble and NH creep) reduces the creep life of the material with increasing stress level from 69.4 to 103.4 MPa, highlighting that creep activation energy largely influences the creep life of single-phase ɤ-TiAl alloy at 832°C.

6. Future work to be done

Extensive TEM-based microstructural investigations are required to further validate the observations obtained from creep curves and correlate the different creep mechanisms with the arrangement of both dislocations and superdislocations during the different creep regimes for both uninterrupted and interrupted creep testing at 832°C. This would provide an experimental evidence for understanding the influence of creep activation energy on the creep life of single-phase ɤ-TiAl alloy.

Acknowledgments

MS would like to acknowledge the Department of Metallurgical and Materials Engineering, NIT Durgapur, for detailed discussions during the preparation of the manuscript.

Disclosure statement

No potential conflict of interest was reported by the author(s).

ORCID

Mainak Saha http://orcid.org/0000-0001-8979-457X

References

[1] Kim YW. Intermetallic alloys based on gamma titanium aluminide. JOM. 1989 Jul;41 (7):24–30. .
[2] Kim SW, Hong JK, Na YS, et al. Development of TiAl alloys with excellent mechanical properties and oxidation resistance. Mater Des. 2014Feb;54:814–819.
[3] Kassner ME. Fundamentals of creep in metals and alloys: third edition. Elsevier Inc; 2015.
[4] Hayes RW, Martin PL. Tension creep of wrought single phase γ TiAl. Acta Metallurgica Et Materialia. 1995 Jul;43(7):2761–2772. .
[5] Huang SC, Hall EL. Plastic deformation and fracture of binary TiAl-base alloys. Metall Trans A. 1991 Feb;22(2):427–439. .
[6] Karthikeyan S, Viswanathan GB, Gouma PI, et al. Mechanisms and effect of microstructure on creep of TiAl-based alloys. Mater Sci Eng A. 2002Jun;329–331:621–630.
[7] Liu CT, Schneibel JH, Maziasz PJ, et al. Tensile properties and fracture toughness of TiAl alloys with controlled microstructures. Intermetallics. 1996 Sep;4(6):429–440. .

Electronic copy available at: https://ssrn.com/abstract=4067222

[8] Hayes R, London B. On the creep deformation of a cast near Gamma TiAl Alloy Ti-48Al-1Nb. Acta Metallurgica et Materialia. cited 2020 Sep 16. 1992 Sep;409:2167–2175. https://digitalcommons.calpoly.edu/mate_fac/106
[9] Chokshi AH. Grain boundary processes in strengthening, weakening, and superplasticity. Adv Eng Mater. 2020 Jan;22(1):1900748. .
[10] Gifkins RC, Langdon TG, McLean D. Grain-Boundary Sliding and Axial Strain during Diffusional Creep. Metal Sci. 1975 Jan;9(1):141–144. .
[11] Mukherjee AK. An examination of the constitutive equation for elevated temperature plasticity. Mater Sci Eng A. 2002 Jan;322(1–2):1–22. .
[12] Mishra RS, Mukherjee AK. On superplasticity in silicon carbide reinforced aluminum composites. Scripta Metallurgica et Materiala. 1991 Feb;25(2):271–275.
[13] Bieler TR, Mishra RS, Mukherjee AK. Superplasticity in hard-to-machine materials. Ann Rev Mater Sci. 1996;26(1):75–106.
[14] Sundararajan G. The Monkman-Grant relationship. Mater Sci Eng A. 1989 Jun;112 (C):205–214. .
[15] Menon M, Fang H D. W.-J,of the, and undefined 1994. Creep and stress rupture behavior of an advanced silicon nitride: part III, stress rupture and the Monkman–Grant relationship. Wiley Online Lib. 2020 Sep 16; https://ceramics.onlinelibrary.wiley.com/doi/abs/10.1111/j.1151-2916.1994.tb05397.x
[16] Saha M. A brief discussion on the tensile creep deformation behaviour of wrought single-phase γ-TiAl. Mater Today Proc. Jan 2021. DOI:10.1016/j.matpr.2020.11.189..
[17] Edwards TEJ, Di Gioacchino F, Goodfellow AJ. Deformation of lamellar γ-TiAl below the general yield stress. Acta Materialia. 2019Jan;163:122–139.
[18] MONKMAN and F. C. An empirical relationship between rupture life and minimum creep rate in creep rupture tests. Proc ASTM. cited 2020 Sep 16. 1956;56:91–103. https://ci.nii.ac.jp/naid/10006401917.
[19] Smallman RE, Ngan AHW Creep, fatigue and fracture. In: Modern physical metallurgy. Elsevier; 2014. p. 571–616.
[20] Smallman RE, Bishop RJ Mechanical behaviour of materials. In: Modern physical metallurgy and materials engineering. Elsevier; 1999. p. 197–258.
[21] Gladysz GM, Chawla KK Intrinsic voids, ideal materials, and real materials. In: Voids in Materials. Elsevier; 2015. p. 13–35.
[22] Cheepu M, Kumar Reddy YA, Indumathi S, et al. Laser welding of dissimilar alloys between high tensile steel and Inconel alloy for high temperature applications. Adv Mater Process Technol. 2020 Dec;1–12. DOI:10.1080/2374068x.2020.1855389.
[23] Mahalle G, Kotkunde N, Gupta AK, et al. Prediction of flow stress behaviour by materials modelling technique for Inconel 718 alloy at elevated temperature. Adv Mater Process Technol. 2020 Apr;6(2):456–463. .
[24] Kumar S, Singh R, Hashmi MSJ. Metal matrix composite: a methodological review. Adv Mater Process Technol. 2020 Jan 2;6(1):13–24. . Taylor and Francis Ltd.
[25] Edward GH, Ashby MF. Intergranular fracture during power-law creep. Acta Metall. 1979;27(9):1505–1518.
[26] Mistler RE, Coble RL. Rate-Determining species in diffusion-Controlled processes in Al2O3. J Am Ceram Soc. 1971;54(1):60–61.
[27] LANGDON TG. Activation energies for creep of pyrolytic and glassy carbon. Nat Phys Sci. 1972 Mar;236(65):60. .
[28] Weertman J. Steady-State creep through dislocation climb. J Appl Phys. 1957;28 (3):362–364.
[29] Nabarro FRN. Steady-state diffusional creep. Philos Mag. 1967;16(140):231–237.
[30] Mohamed FA, Langdon TG. Deformation mechanism maps: their use in predicting creep behavior. J Eng Materi Technol Trans ASME. 1976;98(2):125–130.
[31] Langdon TG, Cropper DR, Pask JA. Creep mechanisms in ceramic materials at elevated temperatures. In: Ceramics in severe environments. US: Springer; 1971. p. 297–313.

Electronic copy available at: https://ssrn.com/abstract=4067222

[32] Yamakov V, Wolf D, Phillpot SR, et al. Grain-boundary diffusion creep in nanocrystalline palladium by molecular-dynamics simulation †. Acta Materialia. 2020 Sep 30. 2002;50 (1):61–73. www.elsevier.com/locate/actamat
[33] Langdon TG. Grain boundary deformation processes. In: Deformation of ceramic materials. US: Springer; 1975. p. 101–126.
[34] Hayes RW, London B. On the creep deformation of a cast near gamma TiAl alloy Ti48Al1 Nb. Acta Metallurgica Et Materialia. 1992;40(9):2167–2175.
[35] Lu M, Hemker KJ. Intermediate temperature creep properties of gamma TiAl. Acta Materialia. 1997 Sep;45(9):3573–3585. .
[36] Viguier B, Hemker KJ. Characterizing faulted dipoles in deformed gamma TiAl. Philosophical Magazine A: Physics of Condensed Matter, Structure, Defects and Mechanical Properties. 1996;73(3):575–599.
[37] Appel F, Wagner R. Microstructure and deformation of two-phase γ-titanium aluminides. In: Materials science and engineering R: reports. Vol. 225 Elsevier; BV 187–268May1 1998.
[38] Hug G, Loiseau A, Lasalmonie A. Nature and dissociation of the dislocations in TiAl deformed at room temperature. Philosophical Magazine A: Physics of Condensed Matter, Structure, Defects and Mechanical Properties. 1986;54(1):47–65.
[39] Fivel MC, Louchet F, Viguier B, et al., "On the stress anomaly of γ-TiAl," in *Materials Research Society Symposium - Proceedings*, 2001, vol. 646, doi: 10.1557/proc-646-n7.10.1.
[40] Louchet F, Viguier B. Modelling the flow stress anomaly in γ-TiAl II. The local pinning-unzipping model: statistical analysis and consequences. Philosophical Magazine A: Physics of Condensed Matter, Structure, Defects and Mechanical Properties. 1995;71(6):1313–1333.

Electronic copy available at: https://ssrn.com/abstract=4067222